Centrosome centering and decentering by microtubule network rearrangement

Gaëlle Letort[1]*, Francois Nedelec[2], Laurent Blanchoin[1,3] and Manuel Théry[1,3]*

1- CytoMorpho Lab, Biosciences & Biotechnology Institute of Grenoble, UMR5168, CEA/INRA/CNRS/Université Grenoble-Alpes, Grenoble, France.
2- Cell Biology and Biophysics Unit, European Molecular Biology Laboratory, Heidelberg, Germany.
3- CytoMorpho Lab, Hopital Saint Louis, Institut Universitaire d'Hematologie, UMRS1160, INSERM/Université Paris Diderot, Paris, France.

*correspondence : gaelle.letort.gl@gmail.com, manuel.thery@cea.fr

Abstract

The centrosome is positioned at the cell center by pushing and pulling forces transmitted by microtubules (MTs). Centrosome decentering is often considered to result from asymmetric, cortical pulling forces exerted in particular by molecular motors on MTs, and controlled by external cues affecting the cell cortex locally. Here we used numerical simulations to investigate the possibility that it could equally result from the redistribution of pushing forces due to a reorientation of MTs. We first showed that MT gliding along cell edges and pivoting around the centrosome regulate MT rearrangement and thereby direct the spatial distribution of pushing forces, while the number, dynamics and stiffness of MTs determine the magnitude of these forces. By modulating these parameters, we identified different regimes, involving both pushing and pulling forces, characterized either by robust centrosome centering, robust off-centering or "reactive" positioning. In those latter conditions weak asymmetric cues can induce a misbalance of pushing and pulling forces resulting in an abrupt transition from a centered to an off-centered position. Altogether these results point at the central role played by the configuration of the MTs on the distribution of pushing forces that position the centrosome. We suggest that asymmetric external cues should not be seen as direct driver of centrosome decentering and cell polarization, but rather as inducers of an effective reorganization of the MT network, fostering centrosome motion to the cell periphery.

Introduction

In many cells, the centrosome is positioned at the geometric center of the cell, across a wide range of conditions: in cultured cells (Burakov et al., 2003), whether they have circular or elongated shapes (Hale et al., 2011), symmetric or asymmetric adhesion patterns (Théry et al., 2006), in migrating cells (Dupin et al., 2009; Gomes et al., 2005), or in fertilized eggs (Kimura and Kimura, 2011a; Minc et al., 2011; Wühr et al., 2010). The robustness of this centering mechanism has been proposed to rely on the contribution of several types of mechanical forces acting on the MTs by pushing and pulling on cytoplasmic organelles and on cell borders, all contributing to stabilize the centrosome at the cell center (Laan et al., 2012a; Zhu et al., 2010). However, in vivo, the centrosome is mostly found at the cell periphery (Tang and Marshall, 2012). Indeed, in most differentiated cells the centrosome is anchored to the plasma membrane, where it serves as a structural base for the primary cilium (Reiter et al., 2012). This simple consideration suggests that the centrosome-MT networks not only have robust centering properties but also efficient off-centering capacities. A global understanding of MT network geometry and centrosome positioning should therefore include the striking ability of this system to easily switch from a centering to an off-centering regime.

External cues are usually considered as the main driver of centrosome off-centering. Indeed, centrosome displacement to the cell periphery can be triggered by an asymmetric cue such as the contact with a neighboring cell (Rodriguez-Fraticelli et al., 2012) or a target cell (Yi et al., 2013) . This cue generally induces local MT capture and the development of tension forces pulling the centrosome toward the cue (Combs et al., 2006; Kozlowski et al., 2007; Nguyen-Ngoc et al., 2007). However, such a mechanism naively requires the off-centering force associated to the asymmetric signal to be strong enough to overcome the centering forces in order to displace the centrosome up to the cell periphery. In such a scenario cells would not respond to minor changes in their environment.

Here we explore the possibility that the centrosome-MT network can adopt more "reactive" conformations in which centrosome position is stable but easily destabilized by a small change in MT organization. In such a state, the centrosome is the converging point of centering and off-centering forces of comparable strength. Therefore a mild change in an intrinsic critical parameter, or a small external cue, can be sufficient to trigger network reorganization and thus bias the force balance so that the off-centering forces win over and move the centrosome to the periphery.

Minus-end directed motors, such as dyneins molecules, produce pulling forces along MT length when bound to cytoplasmic vesicles or selectively on MTs tips when bound to the cell cortex (Kimura and Kimura, 2011b). The cytoplasmic localization of dyneins undoubtedly leads to a net centering force since MTs that are longer on the side of the centrosome that is facing the more distant cell edge are pulled stronger than MTs facing the closest cortex. The cytoplamic pulling scenario also includes adherent cultivated mammalian cell with a flat ('fried egg') geometry, where motors, anchored on the basal surface of the cell, can pull microtubules all along their side. The contribution of dyneins anchored at the cell cortex is less clear. Cortical dyneins may have opposite effects on an isotropic radial array of MTs depending on MTs length distribution and dyneins density relative to MTs (Laan et al., 2012b). MT pushing forces, generated by MT polymerization against the cell periphery, could also center or decenter the centrosome, depending on whether MT tips can slide or not on the cortex and affect the overall network symmetry (Brito et al., 2005; Faivre-

Moskalenko and Dogterom, 2002; Holy et al., 1997; Pinot et al., 2009; Tran et al., 2001). The question of centrosome positioning has been previously explored with coarse-grained models (Ma et al., 2014; Minc et al., 2011; Théry et al., 2007; Zhu et al., 2010). With this approach, individual microtubules are not represented, and the force on the centrosomes is calculated as a sum of elementary forces calculated for each angular sectors of the cell seen from the centrosome. This approach assumes that microtubules are straight, and that the ones reaching the cortex do so in the line-of-sight from the centrosome. Typically, molecular motor are also not represented, and one assumes that their contribution results either in a constant force, in the case where motors pull MT at their tip, or in a force that is proportional to the distance between the centrosome and the cortex, for motors pulling MTs on their side. Pushing forces are assumed to act purely radially, and often to be equal to the threshold for Euler-type buckling. Under these assumptions the resulting equations can be analyzed simply. In other words, MTs were generally assumed to be no longer than the cell size, and their deformation is not considered to depart from a straight configuration. This condition might hold for cells in a mitotic state but not during interphase where MTs can be much longer, and must bend to fit within the cell. This condition makes the coarse-grained approach impractical, but with modern computer hardware and state of the art simulation methods, it is possible to consider every MT explicitly, and solve the system correctly (Maly and Maly, 2010; Pinot et al., 2009; Wu et al., 2011).

To explore the balance between off-centering and centering forces, and tentatively reveal some relevant cellular parameters that would be interesting to focus on experimentally, we used numerical simulations. This approach allowed us to consider the effect of several factors, which are likely to contribute to the regulation of force distribution. We examined microtubule bending and reorientation, and basic parameters, such as MT number, polymerization dynamics and stiffness, on their ability to break MT network symmetry. In this way we identified the possible changes in network architecture that may misbalance pushing and pulling forces and promote centrosome decentering.

Results

Centrosome positioning mechanisms are challenging to study as numerous factors such as cell shape, MTs properties or interacting proteins intervene and vary in different cell types and experimental conditions. Furthermore, there is currently no experimental way to measure the mechanical forces experienced by MTs *in vivo*, or in an *in vitro* assay, precluding the mapping of the spatial distribution of pushing and pulling forces that can be used for centering. Here, simulations were performed with the cytoskeleton simulation dedicated software Cytosim (Nedelec and Foethke, 2007). It is based on Langevin dynamics approach and offers the possibility to take into account numerous components in minimal computational time thanks to semi-implicit numerical integration (Kozlowski et al., 2007; Loughlin et al., 2010, 2011; Ward et al., 2014).

We simulated pure centrosomal arrays, in which all MTs are attached to a common center at their minus ends. The angular distribution of MT nucleation was isotropic. Unless specified, all simulations contained on centrosome composed of 100 MTs simulated for 400 s. MT growth followed the classical two-states dynamic instability model (see supplementary table 1 and Material and Methods for all numerical parameters). MTs were confined to regular geometries representing cell shape. They could bend as linear elastic beams, and thus follow Euler's buckling theory. Entities that could bind/unbind and move along MTs were added to simulate the action of minus end directed motors. Centrosome displacement was limited with an effective drag caused by cytoplasmic viscosity. MTs' growth against geometrical boundaries produced pushing forces whereas minus-end directed motors generated the pulling forces. By simply monitoring the position of the centrosomes, we could deduce if the tested conditions resulted in a net centering or a decentering effect.

Contribution of pulling forces

We first compared the two scenarios in which motors such as dynein molecules are either distributed in the cytoplasm (Figure 1A) or anchored at the cortex (Figure 1B), in a situation where MTs can be longer than the cell radius. In both cases, centrosome moved towards the cell center regardless of the number of dyneins (except in the absence of motors) (Figure 1C). Cortical distribution gave rise to a much faster centrosome motion (Figure 1C). However, it should be noted that the simulations were done for an equal number of dyneins for both distributions, leading thus to highly different local densities.

To further investigate the effect of the cellular geometry on centrosome positioning, we switched to ellipsoidal, rectangular and triangular geometries. We explored the two fundamental motor distributions, systematically varying the total number of motors in the system to explore different ratio of motors to MTs. In the case of cytoplasmic localization of dyneins, the centrosome moved toward the center of gravity of the shape for any given initial position and all tested geometries (Figure 2A), consistent with experimental observation in sea urchin eggs (Minc et al., 2011). In contrast, in the case of a cortical distribution, centrosomes did not move toward the center of gravity in the triangular geometries. After fast and erratic displacements throughout the cell, the centrosome usually converged toward the middle of the longest edge, which contains more dyneins (Figure 2B, C). Like in the circular geometry, the cortical distribution led to stronger net forces as illustrated by faster centrosome displacements (Figure 2C). These results showed how uneven angular

distribution of cortical dyneins can act as a strong decentering force whereas in the case of cytoplasmic dyneins the net force was weaker and systematically directed toward the cell center.

Contribution of pushing forces

MTs generate pushing forces as they polymerize against a barrier (Dogterom and Yurke, 1997). The spatial distribution of growing MTs within the cell impact the direction of the net pushing force exerted on the centrosome. If the aster is isotropic, pushing forces are directed toward the centrosomes, but they are directed away from it in the case of anisotropic distribution (Pavin et al., 2012). Therefore, any parameters influencing MTs spatial distribution, such as nucleation, dynamics or forces that induce bending are likely to play key roles in determining the direction of the net pushing force on the centrosome. MTs are in particular easily deflected by forces applied on their ends. The net force on the centrosome will depend on MT stiffness, the number of MTs and their configurations.

To investigate these effects, we considered a radial array of flexible MTs with their minus-end anchored at the centrosome. MTs are anchored at regular angular intervals, such as to form an isotropic aster, but we tuned the angular stiffness of their anchorage, to allow them to pivot at various degree around their minus-end anchorage. In the basic setup, plus-ends could glide along the edge of the cell, as the contact is considered to be frictionless, but by adding immobile anchors at the cortex, that capture the plus-ends and pin them we can also prevent sliding. Thus varying the angular stiffness at the centrosomes, and the number of anchors points at the cortex, enabled us to test the combinatorial effects of allowing or disabling minus-end pivoting and plus-end gliding (Figure 3A). At first, those simulations were performed in the absence of minus-end motor associated pulling forces. As expected from MT observation in lymphoblastic cell lines (Bornens et al., 1989) and previous numerical simulations (Pinot et al., 2009), when both pivoting and gliding were allowed the network became asymmetric and pushed the centrosome off-center toward the closest edge (Figure 3A, top left). Indeed, MTs oriented toward the closest side were the first to reach the cortex and glide toward the opposite direction to minimize the bending energy associated to their curvature. This effect was limited when MT pivoting was forbidden as it reduced network asymmetry (Figure 3A, top, right). Strikingly, when MT gliding along the cell cortex was prevented, those first MTs in contact with the cell cortex were pinned and pushed on the centrosome, which get displaced toward the opposite cell edge (Figure 3A, bottom left). MT pivoting ability allowed them to join and form comet-like tail pushing the centrosome as observed in *Dictyostelium* (Brito et al., 2005). Interestingly, when both gliding and pivoting were prevented the network never became asymmetric. The network instead rotated briefly and adopted a vortex-shaped conformation in which the pushing forces directed the centrosome toward the cell center (Figure 3A, bottom left). As we reduced the strength of either the pivoting or the gliding stiffness while fixing the other, the network displayed rapid transition from centering to decentering (Figure 3C). This suggested that the modulation of these parameters can be an efficient way to break network symmetry and place the centrosome near the cell periphery (Figure 3B and 3C). Importantly, these behaviors were independent on centrosome initial position (Figure 3B), meaning that if the centrosome is initially positioned at the cell center, the symmetry in the network will be spontaneously broken either because MT pivot, glide or both, leading to centrosome decentering.

We then studied how MT stiffness, number and length affected these behaviors. In the symmetric conformations of the network, when both MT gliding and pivoting were restricted, centering appeared robust to a decrease in MT number and length (Figure S1). The effects of changing MT stiffness were mild, between 20 and 100 pN/μm2. Very soft MTs could not transmit polymerization forces efficiently, whereas very rigid MTs could not bend after reaching the cortex, in both cases freezing the centrosome motion (Figure S1). If the MT network is allowed to be non-isotropic, due to MT gliding along edges or pivoting around the base, then increasing the number of MTs, either by raising the number of nucleation sites or by decreasing the catastrophe rate, as well as increasing their stiffness, progressively reinforced the net pushing forces and decentered the centrosome (Figure 4). Those parameters are therefore interesting targets if one wants to induce centrosome decentering.

Transitions from centering to off-centering net force.

We then combined the pulling forces due to minus-end directed motors and the pushing forces due to MT polymerization to investigate the potential transition from centering to decentering regimes. Since dynein inhibition has been shown to induce centrosome decentering (Burakov et al., 2003; Wu et al., 2011), we assumed that dynein-associated forces contributed to centering the centrosomes, i.e. that dynein molecules are anchored in the cytoplasm rather than at the cell cortex. We first wanted to know if the centrosomes could spontaneously move off center in the absence of asymmetric cues. We thus tested if a global variation of the MT network properties, such as the parameters described above, could overcome the centering effect of cytoplasmic dyneins and promote centrosome displacement up to a peripheral position.

As described in the first part of this study, in the presence of high concentration of cytoplasmic dyneins (4000 dyneins per cell corresponding to 40 per MT), MT outward pushing forces were not sufficient to overcome the dynein-induced centering effect (Figure 1, 2). Transitions were seen only in cells where the dynein concentration was reduced. In the following simulations we used 100 dyneins per cell (ie 1 per MT). This condition is physiologically relevant since it has been shown that pushing and pulling forces are of comparable magnitude (Zhu et al., 2010). We thus studied the conditions in which variations in MT rigidity, number and catastrophe rate, as well as centrosome pivoting and cortex gliding stiffness, could lead to decentering despite the dynein-induced centering pulling forces.

As MT rigidity increased the net force applied on the centrosome progressively switched from centering to decentering (Figure 5A). However, variations of catastrophe rate and number of MTs, although able to increase pushing forces magnitude (Figure 4), were not able to overcome the centering forces (not shown). This is due to the magnitude of the forces applied to MTs tips, which are such that they induce catastrophe events and thus limit the efficiency of pushing force. However, full transition from centering to decentering behavior, could be observed in smaller cells (of radius 7 μm) where the pushing forces are stronger (because they scale in $1/L^2$ according to Euler's theory) (Figure 5B, C). Reducing drastically the catastrophe rate turned the centering regime into a weak decentering one (Figure 5B). The system was quite sensitive to the number of MTs, and a progressive

transition from centering to decentering occurs as the number of MTs increased (Figure 5C). Varying either centrosome angular stiffness (which affected pivoting) or cortex anchor stiffness (which affected sliding) had even more drastic effects, and could induce abrupt transitions in the position of the centrosome (Figure 5D, E). From these results, the ability of the network to reorganize asymmetrically appears as a key regulator of the force balance at the centrosome.

Noteworthy, these results showed that moderate changes in any of the tested parameters, isolated or in parallel, were often sufficient to induce a complete reversal of situation where the centrosomes is located either at the center or near the periphery of the cell. In the case where the transition is not complete, the parameter change could anyway contribute to prime the network for such a transition. For example, allowing the network to be asymmetric increased the net force on the centrosome. Although when this force is effectively counter balanced by the inward pulling forces exerted by cytoplasmic dynein, it made the reversal more likely to occur if another perturbation is added. For example, the net inward pulling force can be further reduced by additional asymmetric outward pulling forces, such as those exerted along cell-cell contacts. This idea was tested by the addition of external cues, which were simulated by the addition of cortical dyneins within a 60° wide crescent. We then compared the response of a constrained network, in which MT central pivoting and peripheral gliding were forbidden, and the response of a "reconfigurable" network in which pivoting and gliding are allowed, to an increasing strength of asymmetric pulling forces (Figure 6A). The constrained network was less sensitive to asymmetric pulling forces since the pushing from the captured MTs opposed the tension developed by the cortical dyneins (Figure 6A). By contrast, the reorientation of MTs in the "reconfigurable" network, redirected some polymerization forces toward the cortical pulling site (Figure 6B). Thus, the "reconfigurable" network appeared more responsive to external cues, and the centrosome is decentered more readily (Figure 6C). Together these results indicate that several intrinsic parameters of the MT networks such as MT number, rigidity and in particular the ability to reorient MTs is key to modulate the response of the cell. The magnitude and distribution of pushing forces could either lead to robust centering of the centrosome or place it in a reactive conformation, where it can respond to weaker external asymmetric stimulation. Such reactive conformations are characterized by spontaneous symmetry breaking events and centrosome decentering in the absence of asymmetric external cues.

Discussion

The mechanisms regulating centrosome positioning are still under investigation, in particular because different mechanisms can prevail in different cellular conditions (Ma et al., 2014). Here we focused on conditions in which MTs can be longer than the cell diameter, which is the case for adult mammalian cells in interphase (Wu et al., 2011) rather the more usually studied large mitotic cells in embryos (Kimura and Onami, 2007; Minc et al., 2011; Wühr et al., 2010). In this condition, several parameters could regulate the symmetry of MT network architecture, independently of external cues or preexisting asymmetries in boundary conditions such as local capture, stabilization or mechanical forces. MTs number, length and rigidity as well as centrosome stiffness all have the ability to induce a spontaneous network symmetry break and thus lead to centrosome decentering.

Centering capacities are generally considered to result from minus-end-directed motors such as dyneins (Kimura and Kimura, 2011b). Here, by using numerical simulations, we compared the contributions of cytoplasmic and cortical dyneins. We confirmed that cytoplasmic dynein molecules induce robust centrosome centering, whereas cortically anchored dyneins are capable of promoting either centering or decentering depending on cell shape (Ma et al., 2014). Asymmetric pulling forces due to cell shape extension promoted centrosome decentering toward cell longest edge.

Next, we studied how the MT network configuration determined the orientations of pushing forces associated to MT polymerization. When MTs were tightly constrained in space, i.e. if they cannot pivot around their anchor point in the centrosome and if their plus-ends may not glide along the cell edge, they maintain an isotropic distribution and generate centering forces. In contrast, when the MTs are free to pivot or slide, the net pushing force pushes the centrosome toward the periphery. In both scenarios, MTs' stiffness and number could modulate the speed at which the centrosome moves. Thus when pushing forces were opposed by dynein induced pulling forces, modifying the number of MTs or their stiffness could trigger a transition from a regime in which the centrosome is at the center, to a regime in which the centrosome adopts a peripheral position.

Our approach was limited to numerical experiments, investigating some of the theoretical mechanisms that can affect MT architecture and centrosome positioning. Our results pointed at the possible role of several parameters, suggesting experimental investigations.

Centrosome angular anchor stiffness appeared as a critical parameter since small variations from 20 to 5 pN/μm were sufficient to induce an abrupt transition from a centering to a decentering regime (Figure 5E). The parameter, which characterizes the strength of MT anchoring at the centrosome, is not well characterized. MTs can detach from the centrosome in mammalian cells (Alieva et al., 2015; Keating and Borisy, 1999) and were seen to pivot around yeast mitotic spindle poles (Kalinina et al., 2012), but the value of the stiffness has not been measured. The effective pivoting stiffness of a MT with respect to the centrosome is likely to depend primarily on the stiffness of the pericentriolar material in which MTs are embedded. Regulation of pericentriolar material density and crosslinking density (Woodruff et al., 2014), as well as the polymerization of actin filaments nearby (Farina et al., 2015), could possibly affect this stiffness. Moreover, the ability of MTs under tension to tear apart pieces of pericentriolar material during specific phases of the cell cycle suggests that the material stiffness is precisely regulated (Krueger et al., 2010; Megraw et al., 2002; Rusan and Wadsworth, 2005).

Pushing forces naturally scale proportionally with the number of MTs in the aster, and scale inversely with the length of MTs, but these parameters also have a less obvious effect on the network symmetry (Figure 4). These parameters vary a lot from a cell type to the other. They are also widely modulated during cell cycle progression (Piehl et al., 2004). It would be interesting to look at them in more details during centering to decentering transitions such as during epithelial morphogenesis, ciliogenesis or immune synapse formation.

Our simulations confirmed a strong role for MT stiffness, which was expected since MT bending stiffness is a key parameter to the transmission of MT polymerization force produced at the plus-end to the centrosomes attached at the minus-end and thereby regulates the net force on the centrosome. Increasing the MT stiffness is sufficient to switch from a centering to a decentering regime (Figure 5A). Several parameters have been shown to affect MT rigidity (Hawkins et al., 2010) the most common being the presence MT associated proteins that can either increase (Felgner et al., 1997) or decrease (Portran et al., 2013) MT bending stiffness. MT crosslinking molecules can also modulate the apparent stiffness of a bundle (Bathe et al., 2008) and thus affect the system similarly.

Cortical stiffness in our simulations reflects the interaction that MTs have with the cell cortex, and is a property of the cell cortex. MT ability to glide or not along cell cortex was key to network rearrangement, symmetry break and orientation of pushing forces toward cell periphery (Figure 3, Figure 5D). This parameter reflects that MTs could get entangled into a crowded cortical actin network or be physically linked to those filaments (Coles and Bradke, 2015). Plus-ends have been seen to grow or not along cell periphery depending on the presence of filament bundles or branched meshwork suggesting that local actin architectures could regulate MT gliding (Théry et al., 2006). Accordingly, changes in cell adhesion and modifications of the associated cortical actin network could result in MT network rearrangements and finally induce centrosome repositioning.

For the sake of simplicity, several factors were not taken into account in our simulations, notably the contribution of non-centrosomal MTs (Alieva et al., 2015) and kinesins (Cross and McAinsh, 2014) although they contribute to the intrinsic regulation of force production and network reorganization. We also ignored key external contribution such as centrosome and MT interactions with the nucleus (Burakov and Nadezhdina, 2013) and the production of forces by the actin cytoskeleton (Gupton et al., 2002; Waterman-Storer and Salmon, 1997). Importantly as well, we have considered that the cytoplasm was devoid of obstacles, and that MT motions were only hindered by the cell boundaries. The elasticity of the actin network and other obstacles surrounding MTs may however constrain their deformation and significantly increase the magnitude of pushing forces they transmit to the centrosome (Brangwynne et al., 2006; Shan et al., 2012). These important parameters deserve further investigation.

In this work, we studied the ability of the centrosome-MT system to reorganize into asymmetric architectures and reorient the pushing forces toward cell periphery. In physiological conditions the network is rarely isolated as cells contact other cells. These contact represent external cues that affect the MT network within each cell. A MT network spanning the entire cytoplasm can physically integrate all these contributions from the surrounding tissue. In the end, the position of the centrosome results from the spatial integration of peripheral cues, either filtered or amplified, depending on the intrinsic properties of the MT network.

Acknowledgements

This work has been supported by the European Research Commission (Starting Grant 310472), the Agence Nationale de la Recherche (ANR-12-BSV5-0014-02), the Labex Grenoble Alliance for Integrated Structural Cell Biology and a CTBU Grant from CEA to Gaëlle Letort.

Materials and Methods

All simulations are performed using Cytosim (www.cytosim.org). The values used of the main parameters are presented in table 1. The motion of elastic fibers surrounded by a viscous fluid (cytoplasmic viscosity of 1 pN.s/µm² used here (Kole et al., 2005) is calculated following Langevin dynamics (Nedelec and Foethke, 2007). Microtubules are thus subject to Brownian motion with amplitude that is determined by the temperature (k_bT=4.2 pN.nm).

Microtubules dynamics

MTs minus-end are stably anchored to the centrosome. The plus-end undergo dynamic instability (Mitchison and Kirschner, 1984). Each state is implemented in Cytosim as follow:

- polymerization occurs with a speed V_g in the absence of load and decreases exponentially under opposing force as measured (Dogterom and Yurke, 1997):

$$V_g = V_0 . e^{-f/fs}$$

where f is the load, f_s the stall force and V_0 the growth speed of a free filament.

- depolymerisation occurs at a constant speed V_d.
- catastrophe events occurr with a rate τ_c, which is dependent on the growth speed of the fiber:

$$\tau_c = \tau_{stall}/(1 + \left(\frac{\tau_{stall}}{\tau_0} - 1\right)\frac{V_g}{V_0})$$

where τ_{stall} is the rate of catastrophe of a stalled microtubules, which is greater than the rate of catastrophe of a free microtubule τ_0 (Janson et al., 2003).

- rescue events occur at a constant rate τ_r .

Microtubules bending elasticity

Microtubules are modeled as semi-flexible polymers (Nedelec and Foethke, 2007),), and their buckling thus follows Euler's prediction. If the loading is slow, buckling occurs in the first mode, at a threshold of force, which for a length L and a persistence length L_p is:

$$f_b = \pi^2 . k_b . T . L_p / L^2$$

Centrosome

The centrosome is simulated as an aster with a fixed number of microtubules. All MTs are attached to a small bead of radius R, whose mobility (i.e. the inverse of the drag coefficient) is chosen to match the value of the mobility calculated for the centrosome in (Zhu et al., 2010) to take into account of experimental centrosome motion velocities from (Burakov et al., 2003). The microtubules are anchored at the center of the aster with two Hookean links. The first link of stiffness k_a attaches the minus-end of the MTs with the center of the bead. The second link of stiffness k_b attaches a distal point on the surface of the bead, with the point of the MT that is located at distance R from the minus end. The number of distal points on the bead is equal to the number of MTs in the aster, and they are distributed regularly around the center of bead, such as to induce an isotropic aster. To allow MTs to pivot, k_b is set to zero. In this case, MT are only constrained by one link, and can freely pivot while their minus-ends stay attached to the center of the bead.

Confinement

To model the effect of the cortex of the cell on microtubules, the fibers are confined within a fixed geometry. An Hookean force is applied to every microtubule model points that is located outside the confinement geometry:

$$f_c = k_c\,(p(x) - x)$$

where k_c is the spring stiffness and p(x) the projection of the model point x on the confinement space. In addition, microtubules reaching the edge of the geometry can be "pinned" by a spring of stiffness k_g acting between the microtubule plus end and the point at which the plus end first reached the edge. When this constraint is added, then gliding of microtubules along the cortex is strongly impaired.

Motors

Dynein are simulated as a point-like object, that can bind and unbind to microtubules, linked to a fixed anchoring position by a spring of stiffness k_d. This spring represents the anchorage of dyneins either at the cortex or on some vesicle in the cytoplasm. The dynein head moves on a fiber with a speed that depends on the load experienced by the spring:

$$V = V_{max}(1 - \frac{f}{f_{sm}})$$

where V_{max} is the speed of a motor without load and f_{sm} is the motor stall force. The value of V_{max} used here is negative representing the fact that dynein head moves toward the minus end of the microtubule.

Strong cortical motors

Strong cortical motors were added to the simulation to represent the possible effect of local motors associated with proteins such as Par3 in the cortical environment. The particularity of these motors is that they do not unbind from the microtubule unless it is shrinking. Moreover, when they are bound close to the microtubule plus end (within 0.5 μm), they stabilize their plus-end by inhibiting catastrophe events.

Table 1: Default parameters used in the simulations

Microtubules		
Rigidity	25 pN.μm²	Persistence length of 5200 μm (Gittes et al., 1993)
Polymerisation speed	0.13 μm/s	(Burakov et al., 2003)
Depolymerisation speed	-0.27 μm/s	(Burakov et al., 2003)
Rescue rate	0.064 s^{-1}	(Burakov et al., 2003)
Stall force	5 pN	(Dogterom and Yurke, 1997)
Catastrophe rates	0.01 s^{-1}, 0.04 s^{-1}	Free catastrophe rate and stall catastrophe rates. Adapted from (Janson et al., 2003), with higher values for free rate to take into account the absence of cytoplasmic obstacles
Total tubulin	10000	Limited tubulin units available
Centrosome		
Radius	0.5 μm	Radius of centrosome disc
Viscosity	200 pN s/μm²	Constrained centrosome mobility due to friction generated by pericentriolar clous and MTs. Mobility around 0.03 μm/pN/min (Zhu et al., 2010).
First anchoring stiffness	500 pN/μm	Stiffness of first link anchoring MT minus ends to centrosome center
Second anchoring stiffness	0 or 500 pN/μm	Stiffness of second link anchoring MT to centrosome periphery
Number of MTs	100	(Zhu et al., 2010)
Dyneins		
Motion speed	-1.5 μm/s	Bound motor speed without load (Gross et al., 2000)
Stall force	1.1 pN	Maximal force of a dynein (Gross et al., 2000)
Spring stiffness	100 pN/μm	Spring anchoring dynein to its initial position
Confinement space		
Cell radius	10 μm	Default circular geometry
Confinement stiffness	500 pN/μm	Confinement strength of MTs inside the space
Glued stiffness	50 pN/μm	Strength of anchoring MT plus ends to cell cortex when gliding is not allowed

References

Alieva, I.B., Berezinskaya, T., Borisy, G.G., and Vorobjev, I.A. (2015). Centrosome nucleates numerous ephemeral microtubules and only few of them participate in the radial array. Cell Biol. Int. *39*, 1203–1216.

Bathe, M., Heussinger, C., Claessens, M.M. a E., Bausch, A.R., and Frey, E. (2008). Cytoskeletal bundle mechanics. Biophys. J. *94*, 2955–2964.

Bornens, M., Paintrand, M., and Celati, C. (1989). The cortical microfilament system of lymphoblasts displays a periodic oscillatory activity in the absence of microtubules: implications for cell polarity. J. Cell Biol. *109*, 1071–1083.

Brangwynne, C.P., MacKintosh, F.C., Kumar, S., Geisse, N. a, Talbot, J., Mahadevan, L., Parker, K.K., Ingber, D.E., and Weitz, D. a (2006). Microtubules can bear enhanced compressive loads in living cells because of lateral reinforcement. J. Cell Biol. *173*, 733–741.

Brito, D.A., Strauss, J., Magidson, V., Tikhonenko, I., Khodjakov, A., and Koonce, M.P. (2005). Pushing forces drive the comet-like motility of microtubule arrays in Dictyostelium. Mol. Biol. Cell *16*, 3334–3340.

Burakov, A. V, and Nadezhdina, E.S. (2013). Association of nucleus and centrosome: magnet or velcro? Cell Biol. Int. *37*, 95–104.

Burakov, A., Nadezhdina, E., Slepchenko, B., and Rodionov, V. (2003). Centrosome positioning in interphase cells. J. Cell Biol. *162*, 963–969.

Coles, C.H., and Bradke, F. (2015). Coordinating Neuronal Actin–Microtubule Dynamics. Curr. Biol. *25*, R677–R691.

Combs, J., Kim, S.J., Tan, S., Ligon, L.A., Holzbaur, E.L., Kuhn, J., and Poenie, M. (2006). Recruitment of dynein to the Jurkat immunological synapse. Proc Natl Acad Sci U S A *103*, 14883–14888.

Cross, R. a., and McAinsh, A. (2014). Prime movers: the mechanochemistry of mitotic kinesins. Nat. Rev. Mol. Cell Biol. *15*, 257–271.

Dogterom, M., and Yurke, B. (1997). Measurement of the Force-Velocity Relation for Growing Microtubules. Science (80-.). *278*, 856–860.

Dupin, I., Camand, E., and Etienne-Manneville, S. (2009). Classical cadherins control nucleus and centrosome position and cell polarity. J. Cell Biol. *185*, 779–786.

Faivre-Moskalenko, C., and Dogterom, M. (2002). Dynamics of microtubule asters in microfabricated chambers: the role of catastrophes. Proc. Natl. Acad. Sci. U. S. A. *99*, 16788–16793.

Farina, F., Gaillard, J., Guérin, C., Sillibourne, J., Blanchoin, L., and Théry, M. (2015). The centrosome is an actin-organizing center. Under Revis. Nat. Cell Biol.

Felgner, H., Frank, R., Biernat, J., Mandelkow, E., Mandelkow, E., Ludin, B., Matus, A., and Schliwa, M. (1997). Domains of Neuronal Microtubule-associated Proteins and Flexural Rigidity of Microtubules. *138*, 1067–1075.

Gittes, F., Mickey, B., Nettleton, J., and Howard, J. (1993). Flexural rigidity of microtubules and actin filaments measured from thermal fluctuations in shape. J. Cell Biol. *120*, 923–934.

Gomes, E.R., Jani, S., and Gundersen, G.G. (2005). Nuclear movement regulated by Cdc42, MRCK, myosin, and actin flow establishes MTOC polarization in migrating cells. Cell *121*, 451–463.

Gross, S.P., Welte, M.A., Block, S.M., and Wieschaus, E.F. (2000). Dynein-mediated cargo transport in vivo: A switch controls travel distance. J. Cell Biol. *148*, 945–955.

Gupton, S.L., Salmon, W.C., and Waterman-Storer, C.M. (2002). Converging populations of f-actin promote breakage of associated microtubules to spatially regulate microtubule turnover in migrating cells. Curr. Biol. *12*, 1891–1899.

Hale, C.M., Chen, W.-C., Khatau, S.B., Daniels, B.R., Lee, J.S.H., and Wirtz, D. (2011). SMRT analysis of MTOC and nuclear positioning reveals the role of EB1 and LIC1 in single-cell polarization. J. Cell Sci. *124*, 4267–4285.

Hawkins, T., Mirigian, M., Selcuk Yasar, M., and Ross, J.L. (2010). Mechanics of microtubules. J. Biomech. *43*, 23–30.

Holy, T.E., Dogterom, M., Yurke, B., and Leibler, S. (1997). Assembly and positioning of microtubule asters in microfabricated chambers. Proc. Natl. Acad. Sci. U. S. A. *94*, 6228–6231.

Janson, M.E., de Dood, M.E., and Dogterom, M. (2003). Dynamic instability of microtubules is regulated by force. J. Cell Biol. *161*, 1029–1034.

Kalinina, I., Nandi, A., Delivani, P., Chacón, M.R., Klemm, A.H., Ramunno-Johnson, D., Krull, A., Lindner, B., Pavin, N., and Tolić-Nørrelykke, I.M. (2012). Pivoting of microtubules around the spindle pole accelerates kinetochore capture. Nat. Cell Biol. *14*, 1–8.

Keating, T.J., and Borisy, G.G. (1999). Centrosomal and non-centrosomal microtubules. Biol. Cell *91*, 321–329.

Kimura, A., and Onami, S. (2007). Local cortical pulling-force repression switches centrosomal centration and posterior displacement in C. elegans. J. Cell Biol. *179*, 1347–1354.
Kimura, K., and Kimura, A. (2011a). Intracellular organelles mediate cytoplasmic pulling force for centrosome centration in the Caenorhabditis elegans early embryo. Proc. Natl. Acad. Sci. U. S. A. *108*, 137–142.
Kimura, K., and Kimura, A. (2011b). A novel mechanism of microtubule length-dependent force to pull centrosomes toward the cell center. Bioarchitecture *1*, 74–79.
Kole, T.P., Tseng, Y., Jiang, I., Katz, J.L., and Wirtz, D. (2005). Intracellular Mechanics of Migrating Fibroblasts □. Mol. Biol. Cell *16*, 328–338.
Kozlowski, C., Srayko, M., and Nedelec, F. (2007). Cortical microtubule contacts position the spindle in C. elegans embryos. Cell *129*, 499–510.
Krueger, L.E., Wu, J.C., Tsou, M.F.B., and Rose, L.S. (2010). LET-99 inhibits lateral posterior pulling forces during asymmetric spindle elongation in C. elegans embryos. J. Cell Biol. *189*, 481–495.
Laan, L., Pavin, N., Husson, J., Romet-Lemonne, G., van Duijn, M., López, M.P., Vale, R.D., Jülicher, F., Reck-Peterson, S.L., and Dogterom, M. (2012a). Cortical Dynein Controls Microtubule Dynamics to Generate Pulling Forces that Position Microtubule Asters. Cell *148*, 502–514.
Laan, L., Roth, S., and Dogterom, M. (2012b). End-on microtubule-dynein interactions and pulling-based positioning of microtubule organizing centers. Cell Cycle *11*, 3750–3757.
Loughlin, R., Heald, R., and Nedelec, F. (2010). A computational model predicts Xenopus meiotic spindle organization. J. Cell Biol. *191*, 1239–1249.
Loughlin, R., Wilbur, J.D., McNally, F.J., Nedelec, F., and Heald, R. (2011). Katanin Contributes to Interspecies Spindle Length Scaling in Xenopus. Cell *147*, 1397–1407.
Ma, R., Laan, L., Dogterom, M., Pavin, N., and Jülicher, F. (2014). General theory for the mechanics of confined microtubule asters. New J. Phys. *16*.
Maly, V.I., and Maly, I. V. (2010). Symmetry, stability, and reversibility properties of idealized confined microtubule cytoskeletons. Biophys. J. *99*, 2831–2840.
Megraw, T.L., Kilaru, S., Turner, F.R., and Kaufman, T.C. (2002). The centrosome is a dynamic structure that ejects PCM flares. J. Cell Sci. *115*, 4707–4718.
Minc, N., Burgess, D., and Chang, F. (2011). Influence of cell geometry on division-plane positioning. Cell *144*, 414–426.
Mitchison, T., and Kirschner, M. (1984). Dynamic instability of microtubule growth. Nature *312*, 237–242.
Nedelec, F., and Foethke, D. (2007). Collective Langevin dynamics of flexible cytoskeletal fibers. New J. Phys. *9*, 427–427.
Nguyen-Ngoc, T., Afshar, K., and Gönczy, P. (2007). Coupling of cortical dynein and G alpha proteins mediates spindle positioning in Caenorhabditis elegans. Nat. Cell Biol. *9*, 1294–1302.
Pavin, N., Laan, L., Ma, R., Dogterom, M., and Jülicher, F. (2012). Positioning of microtubule organizing centers by cortical pushing and pulling forces. New J. Phys. *14*, 105025.
Piehl, M., Tulu, U.S., Wadsworth, P., and Cassimeris, L. (2004). Centrosome maturation: measurement of microtubule nucleation throughout the cell cycle by using GFP-tagged EB1. Proc. Natl. Acad. Sci. U. S. A. *101*, 1584–1588.
Pinot, M., Chesnel, F., Kubiak, J.Z., Arnal, I., Nedelec, F.J., and Gueroui, Z. (2009). Effects of confinement on the self-organization of microtubules and motors. Curr. Biol. *19*, 954–960.
Portran, D., Zoccoler, M., Gaillard, J., Stoppin-Mellet, V., Neumann, E., Arnal, I., Martiel, J.-L., and Vantard, M. (2013). MAP65/Ase1 promote microtubule flexibility. Mol. Biol. Cell *24*, 1964–1973.
Reiter, J.F., Blacque, O.E., and Leroux, M.R. (2012). The base of the cilium: roles for transition fibres and the transition zone in ciliary formation, maintenance and compartmentalization. EMBO Rep. *13*, 608–618.
Rodriguez-Fraticelli, A.E., Auzan, M., Alonso, M. a, Bornens, M., and Martin-Belmonte, F. (2012). Cell confinement controls centrosome positioning and lumen initiation during epithelial morphogenesis. J. Cell Biol. *198*, 1011–1023.
Rusan, N.M., and Wadsworth, P. (2005). Centrosome fragments and microtubules are transported asymmetrically away from division plane in anaphase. J. Cell Biol. *168*, 21–28.
Shan, W.L., Chen, Z., Broedersz, C.P., Gumaste, a. a., Soboyejo, W.O., and Brangwynne, C.P. (2012). Attenuated short wavelength buckling and force propagation in a biopolymer-reinforced rod. Soft Matter 194–199.
Tang, N., and Marshall, W.F. (2012). Centrosome positioning in vertebrate development. J. Cell Sci. *125*, 4951–4961.

Théry, M., Racine, V., Piel, M., Pépin, A., Dimitrov, A., Chen, Y., Sibarita, J.-B., and Bornens, M. (2006). Anisotropy of cell adhesive microenvironment governs cell internal organization and orientation of polarity. Proc. Natl. Acad. Sci. U. S. A. *103*, 19771–19776.

Théry, M., Jiménez-Dalmaroni, A., Racine, V., Bornens, M., and Jülicher, F. (2007). Experimental and theoretical study of mitotic spindle orientation. Nature *447*, 493–496.

Tran, P.T., Marsh, L., Doye, V., Inoué, S., and Chang, F. (2001). A Mechanism for Nuclear Positioning in Fission Yeast Based on Microtubule Pushing 7. *153*, 397–411.

Ward, J.J., Roque, H., Antony, C., and Nedelec, F. (2014). Mechanical design principles of a mitotic spindle. Elife *3*, 1–28.

Waterman-Storer, C.M., and Salmon, E.D. (1997). Actomyosin-based retrograde flow of microtubules in the lamella of migrating epithelial cells influences microtubule dynamic instability and turnover and is associated with microtubule breakage and treadmilling. J. Cell Biol. *139*, 417–434.

Woodruff, J.B., Wueseke, O., Hyman, A.A., and B, P.T.R.S. (2014). Pericentriolar material structure and dynamics Pericentriolar material structure and dynamics.

Wu, J., Misra, G., Russell, R.J., Ladd, A.J.C., Lele, T.P., and Dickinson, R.B. (2011). Effects of dynein on microtubule mechanics and centrosome positioning. Mol. Biol. Cell *22*, 4834–4841.

Wühr, M., Tan, E.S., Parker, S.K., Detrich, H.W., and Mitchison, T.J. (2010). A model for cleavage plane determination in early amphibian and fish embryos. Curr. Biol. *20*, 2040–2045.

Yi, J., Wu, X., Chung, A.H., Chen, J.K., Kapoor, T.M., and Hammer, J. a (2013). Centrosome repositioning in T cells is biphasic and driven by microtubule end-on capture-shrinkage. J. Cell Biol. *202*, 779–792.

Zhu, J., Burakov, A., Rodionov, V., and Mogilner, A. (2010). Finding the Cell Center by a Balance of Dynein and Myosin Pulling and Microtubule Pushing : A Computational Study. Mol. Biol. Cell *21*, 4418–4427.

Figure legends

Figure 1

Distribution of pulling forces: effect on centrosome centering.

(A-C) Centrosome position is indicated by colored points, from blue (0 s) to red (400 s). Dynein are shown in green and MTs in white in simulation snapshots. (A) Cytoplasmic distribution of motors. (left) Time snapshots of one simulation. (right) Centrosome trajectory in the cell over time on the simulation shown in the left panel. Grey area represents the cell area filled by motors. (B) Cortical distribution of motors. (left) Time snapshots of one simulation. (right) Centrosome trajectory in the cell over time on the simulation shown in the left panel. Grey outline represents the cell cortex filled by motors. (C) Variation of the number of motors for both motor distribution. Trajectories of 15 simulations for (left) the cytoplasmic distribution and (middle) the cortical distribution. Number of simulated dyneins is increased from left to right in the arc axis from 0 to 7000 with a step of 500. Initially centrosome are placed along the arc axis which is at half the cell radius. (Right) Maximal speed reached by centrosome during each simulation according to the number of dyneins for cytoplasmic (full line with full points) and cortical (dashed line with empty points) distributions.

Figure 2

Distribution of pulling forces in different cell geometries.

(A-B) (top) Snapshot of final time (400 s) of one simulation for different geometries: ellipse, rectangle, equilateral triangle, isocele triangle whose base is the smallest side and isocele triangle whose base is the longest side. Dynein are shown in green, MTs in white and centrosome in gray. Motors are either distributed (A) cytoplasmically or (B) cortically (bottom) Trajectories of centrosome in 15 simulations for each geometry. Centrosome position is indicated by colored points, from blue (0 s) to red (400 s) in the trajectories plots. Gray area represents the motor spreading area. Black dot indicates the cell gravity center. (C) (left) Boxplot of the distance of centrosome to gravity center at the end of the simulation for each geometries, for cytoplasmic (full boxes) and corticall (empty boxes) distributions. (right) Stripchart of the final speed of centrosome in the simulations for each geometries for cytoplasmic (full triangles) and cortical (empty triqngles) distributions.

Figure 3

Pushing forces: MT network topology effect.

(A) (left) schematic representation of (top) MT gliding ability and (bottom) MT pivoting ability. MTs and centrosomal complex are in green, actin cortex in red. (right) Snapshots of final state (400 s) of simulation for each one of the condition: pivoting allowed or not and gliding allowed or not. (B) Trajectories of centrosome in 15 simulations with different initial distances to cell center for each of the pivoting/gliding conditions. Black point indicates cell gravity center. (C) (left) Trajectories of centrosome in simulations with varying pivoting stiffness when gliding is not allowed. Pivoting stiffness is varied exponentially from 0 to 150 pN/μm from left to right on the arc axis. (right) Final distance of centrosome to cell center in the simulations according to the pivoting stiffness. Dashed-line indicates the initial centrosome-center distance. (D) (left) Trajectories of centrosome in simulations with varying gliding stiffness when pivoting is not allowed. Gliding stiffness is varied exponentially from 0 to 15.5 pN/μm from left to right on the arc axis. (right) Final distance of centrosome to cell center in the simulations according to the gliding stiffness. Dashed-line indicates

the initial centrosome-center distance. (A-D) Centrosome position is indicated by colored points, from blue (0 s) to red (400 s) in the trajectories plots.

Figure 4

Efficiency of pushing forces (with pivoting and gliding allowed).

(A-C) (left) Snapshots of final time (400 s) of one simulation for 2 different conditions for each varying parameter. (middle) Trajectories of simulations with varying parameter along the arc axis, increasing from left to right. Centrosome position is indicated by colored points, from blue (0 s) to red (400 s). Cell center is indicated by a black point. (right) Final distance of centrosome to cell center according to the varying parameter. Dashed-line represents the initial centrosome-center distance (half the confinement radius). (A) Variation of MT rigidity, from 1 to 300 pN.µm². (B) Variation of MT free catastrophe rate from 0.01 to 0.06 /s. (C) Variation of the number of nucleated MT from 15 to 350.

Figure 5

Transition between centering and off-centering behavior.

(A-E) 100 cytoplasmic dyneins are randomly positioned in the cell. (left) Snapshots of final time (400 s) of one simulation for 2 different conditions for each varying parameter. (middle) Trajectories of simulations with varying parameter along the arc axis, increasing from left to right. Centrosome position is indicated by colored points, from blue (0 s) to red (400 s). Cell center is indicated by a black point. (right) Final distance of centrosome to cell center according to the varying parameter. Dashed-line represents the initial centrosome-center distance (half the confinement radius). (A-C) MTs are allowed to pivote and glide. (A) Variation of MT rigidity, from 1 to 260 pN.µm². (B) Variation of MT free catastrophe rate from 0.01 to 0.06 /s. (C) Variation of the number of nucleated MT from 15 to 350. (D) Variation of MT gliding stiffness when pivoting is not allowed, from 0 to 10 pN/µm. (E) Variation of MT pivoting stiffness when gliding is not allowed, from 0 to 110 pN/µm. Cell radius is 10 µm in (A) and 7 µm in (B-E).

Figure 6

Sensitivity of centrosome positioning to external cues modulated by internal properties.

(A-B) Cell radius is 10 µm. 300 cytoplasmic dyneins are randomly positioned. MT rigidity is set to 15 pN.µm². Centrosome is initially placed in the center of the cell. (A) (left) Snapshots of final simulation time (400 s) in which different number (5, 130, 400 and 800) of cortical dynein have been added on a 60° cressent at the "bottom" part of the cell. (right) Trajectories of centrosome in the cell. Colors represent the number of dynein used from 0 (green) to 1000 (red). The position of the cortical cressent is shifted to distinguish the different trajectories. (top) MT pivoting and gliding are not allowed. (bottom) MT pivoting and gliding are allowed. (B) (left) schematic representation of MT network configuration when MT pivoting and gliding are not allowed (blue) and both are allowed (purple). Cortical cressent of dynein is represented in black. (right) Final distance of centrosome to cell center according to the number of cortical dynein placed on the cressent, when gliding and pivoting are not allowed (blue) and allowed (purple). The black horizontal dashed-line represents the threshold above which we considered the centrosome as fully off-centered. Colored vertical dashed line represents the threshold number of dyneins necessary to be in off-centering state.

Supplementary figures and movies legends

Figure S1

Pushing forces effect in different cell geometries.

(top) MT pivoting and gliding are allowed. (bottom) MT pivoting and gliding are not allowed.

Snapshot of final time (400 s) of one simulation for different geometries: ellipse, rectangle, equilateral triangle, isocele triangle whose base is the smallest side and isocele triangle whose base is the longest side. Trajectories of centrosome in 15 simulations for each geometry. Centrosome position is indicated by colored points, from blue (0 s) to red (400 s) in the trajectories plots. Black dot indicates the cell gravity center.

Figure S2

Efficiency of pushing forces (with pivoting and gliding not allowed).

(A-C) (left) Snapshots of final time (400 s) of one simulation for 2 different conditions for each varying parameter. (middle) Trajectories of simulations with varying parameter along the arc axis, increasing from left to right. Centrosome position is indicated by colored points, from blue (0 s) to red (400 s). Cell center is indicated by a black point. (right) Final distance of centrosome to cell center according to the varying parameter. Dashed-line represents the initial centrosome-center distance (half the confinement radius). (A) Variation of MT rigidity, from 1 to 300 pN.µm². (B) Variation of MT free catastrophe rate from 0.01 to 0.06 /s. (C) Variation of the number of nucleated MT from 15 to 350.

Movie S1

Pulling forces distribution. Simulation for 400 s for cytoplasmic (left) and cortical (right) dynein distributions in circular geometry.

Cell radius is 10 µm. 4000 dynein are uniformly distributed.

Movie S2

Pulling forces distribution in different geometries. Simulation for 400 s for cytoplasmic (top) and cortical (bottom) distributions. Differents geometires are used (from left to right): ellipse, rectangle, equilateral triangle, isocele triangle with base being the smallest side and isocele triangle whose base is the longest side. Geometries area are kept constant around 314 µm². 4000 dyneins are positioned.

Movie S3

Pushing forces: MT network topology effect. Simulations for 400 s of MT dynamics with no motors, when MT gliding is allowed (top row) or not (bottom row), and pivoting is allowed (left column) or not (right column). Cell radius is 10 µm.

Movie S4

Pushing forces: variation of MT parameters. Simulations for 400 s for varying MT properties: MT rigidity (top row), MT catastrophe rate (middle row) and MT number (bottom row). MTs are allowed to pivote and glide. Cell radius is 10 µm.

Movie S5

Pushing forces: variation of MT parameters. Simulations for 400 s for varying MT properties: MT rigidity (top row), MT catastrophe rate (middle row) and MT number (bottom row). MTs are not allowed to pivote and glide. Cell radius is 10 μm.

Movie S6

Balance between pushing and pulling forces. Simulations for 400 s with few (100) cytoplasmic dyneins with varying MT properties: MT rigidity (top left, pivoting and gliding allowed), MT catastrophe rate (middle left, pivoting and gliding allowed), MT number (bottom left, pivoting and gliding allowed), MT gliding stiffness (top right, pivoting not allowed) and MT pivoting stiffness (bottom right, gliding not allowed). Cell radius is 10 μm when varying MT rigidity (top left) and 7 μm otherwise. Dynein are shown in green.

Movie S7

Sensitivity of centering mechanism to external cues.

Simulations for 400 s with few (300) cytoplasmic dyneins (shown in green) with different numbers of asymetrically cortical dyneins added in a 60° cressent at the bottom. Differentce of behavior when MT pivoting and gliding are not allowed (top) or allowed (bottom). Cell radius is 10 μm.

Figure 1

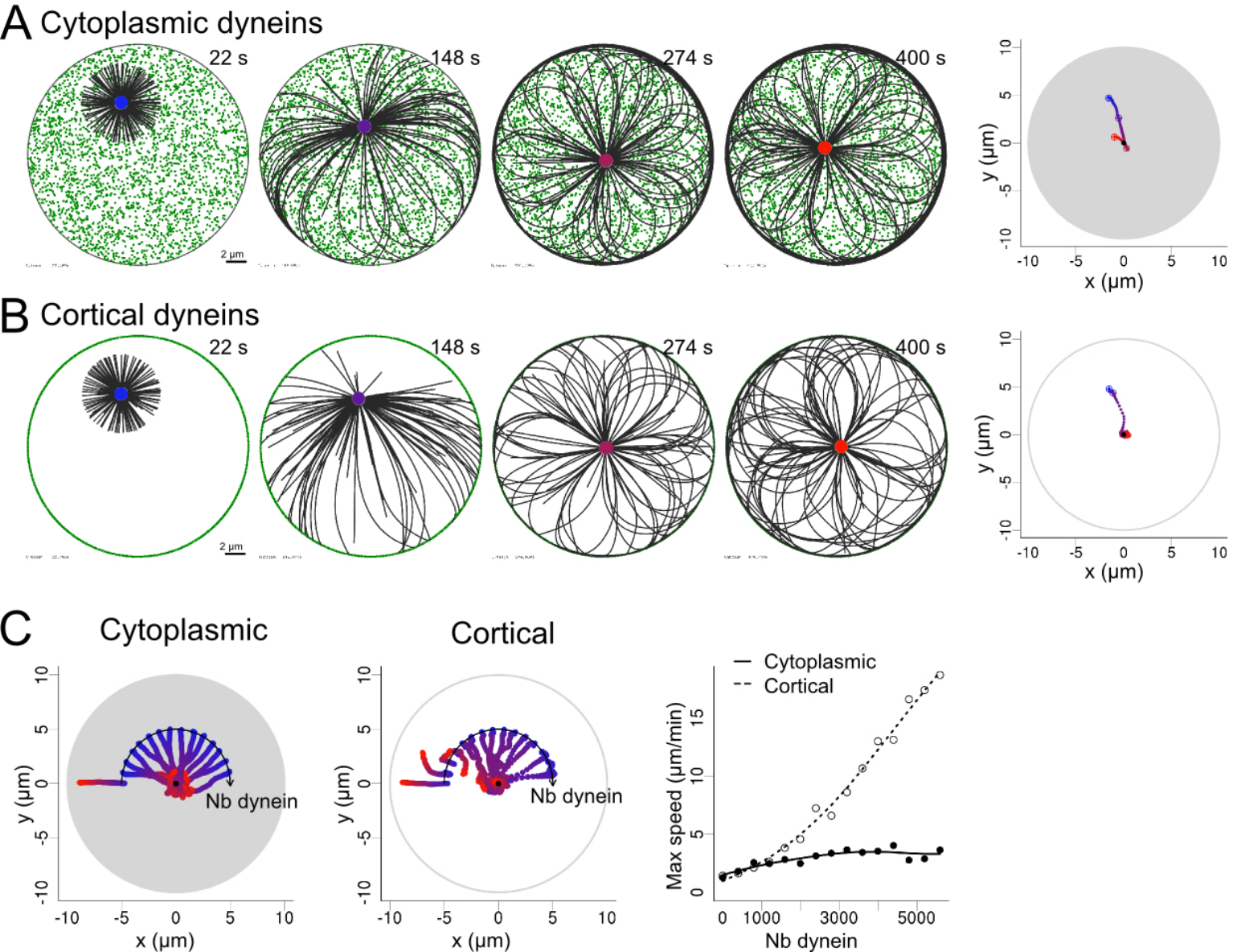
A Cytoplasmic dyneins
22 s
148 s
274 s
400 s
2 µm
y (µm)
x (µm)
B Cortical dyneins
22 s
148 s
274 s
400 s
2 µm
y (µm)
x (µm)
C
Cytoplasmic
Cortical
Nb dynein
Nb dynein
y (µm)
x (µm)
Cytoplasmic
Cortical
Max speed (µm/min)
Nb dynein

Figure 2

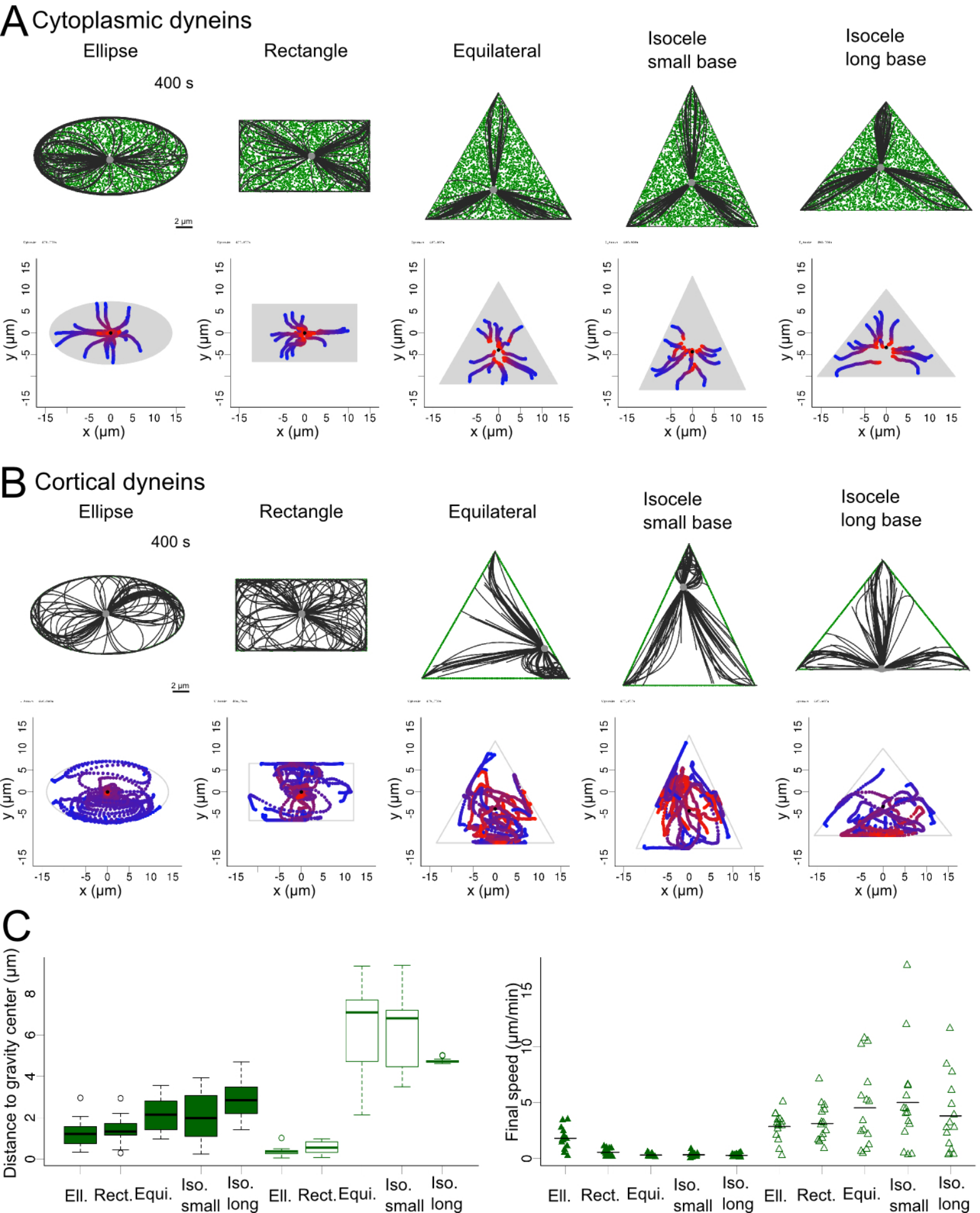
A Cytoplasmic dyneins
Ellipse
Rectangle
Equilateral
Isocele small base
Isocele long base
400 s
2 µm
y (µm)
x (µm)
B Cortical dyneins
Ellipse
Rectangle
Equilateral
Isocele small base
Isocele long base
400 s
2 µm
y (µm)
x (µm)
C
Distance to gravity center (µm)
Ell.
Rect.
Equi.
Iso. small
Iso. long
Final speed (µm/min)

Figure 3

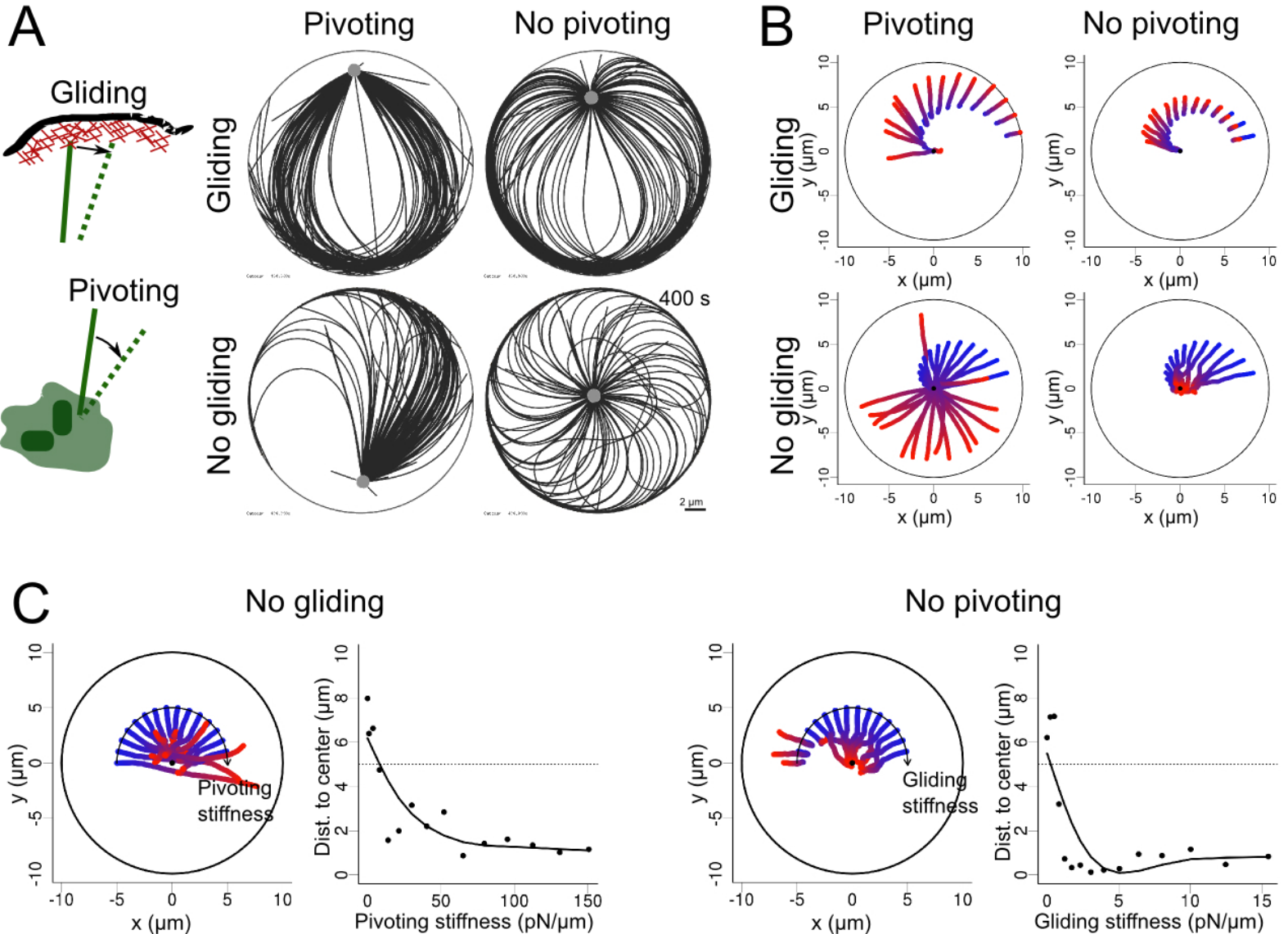
A
Gliding
Pivoting
Pivoting
No pivoting
Gliding
No gliding
400 s
2 µm
B
Pivoting
No pivoting
Gliding
No gliding
x (µm)
y (µm)
C
No gliding
No pivoting
Pivoting stiffness
Gliding stiffness
Dist. to center (µm)
Pivoting stiffness (pN/µm)
Gliding stiffness (pN/µm)

Figure 4

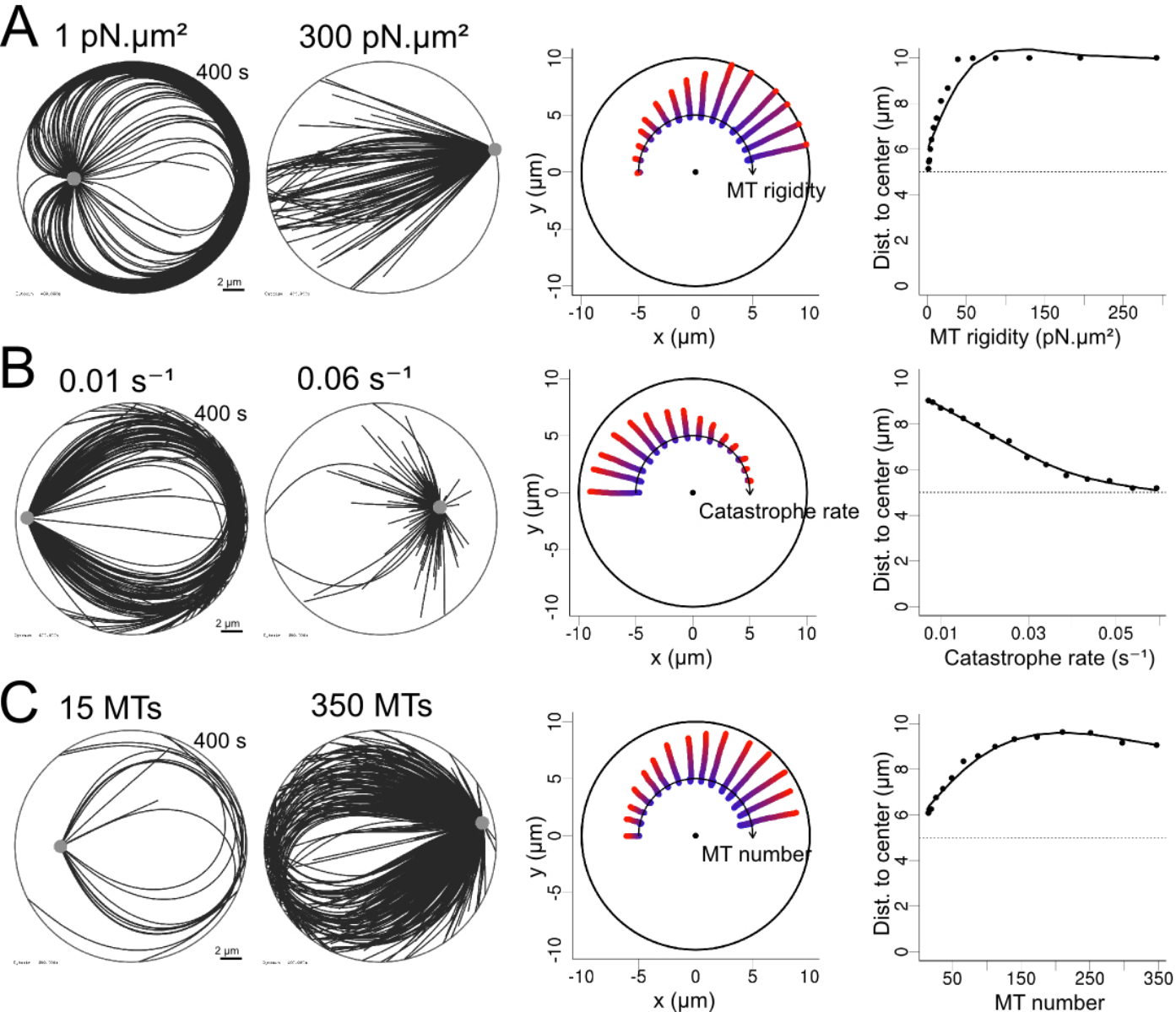
A
1 pN.μm²
300 pN.μm²
400 s
2 μm
MT rigidity
y (μm)
x (μm)
Dist. to center (μm)
MT rigidity (pN.μm²)
B
0.01 s⁻¹
0.06 s⁻¹
400 s
2 μm
Catastrophe rate
y (μm)
x (μm)
Dist. to center (μm)
Catastrophe rate (s⁻¹)
C
15 MTs
350 MTs
400 s
2 μm
MT number
y (μm)
x (μm)
Dist. to center (μm)
MT number

Figure 5

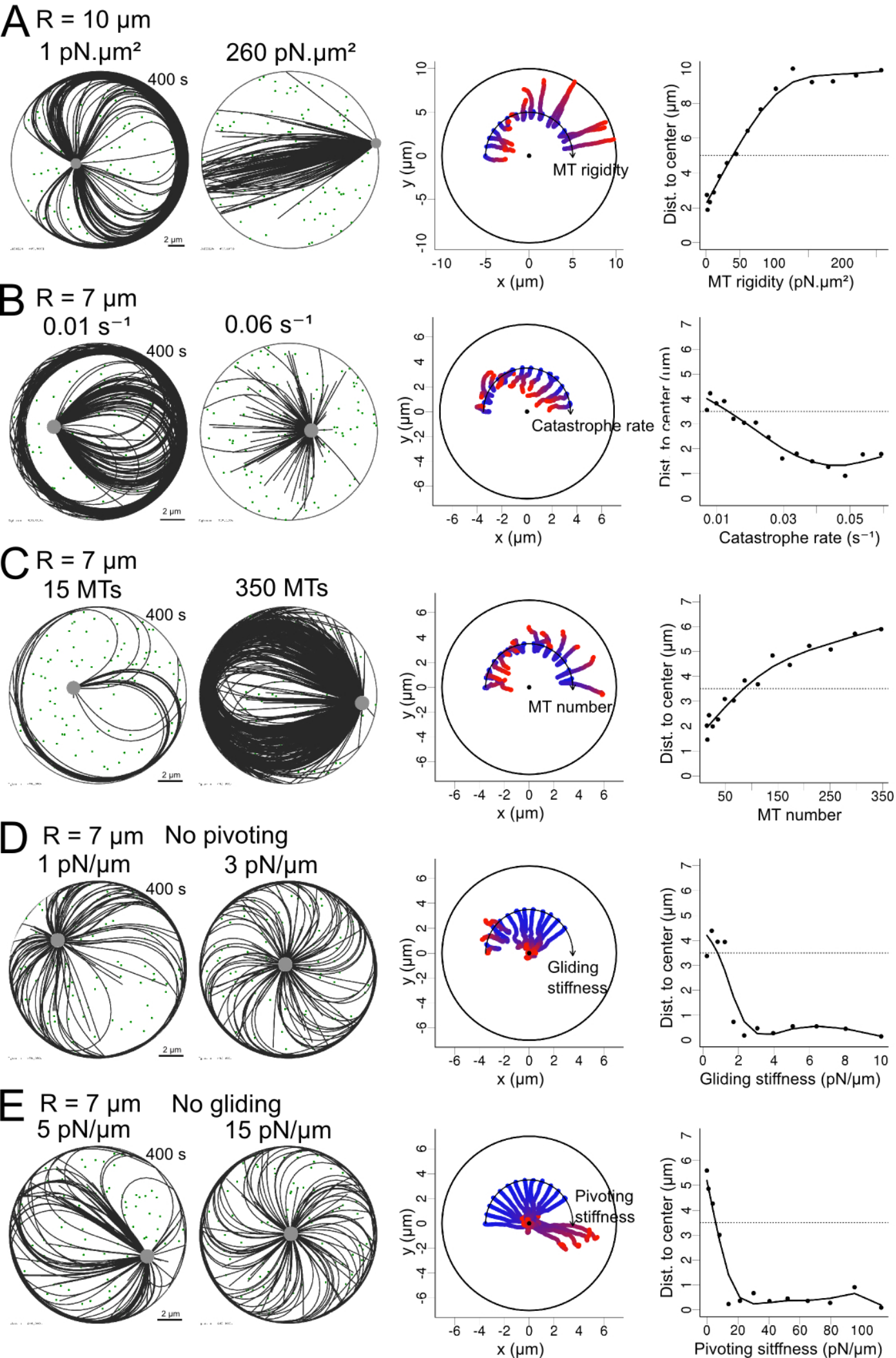
A
R = 10 µm
1 pN.µm²
260 pN.µm²
400 s
2 µm
MT rigidity
x (µm)
y (µm)
Dist. to center (µm)
MT rigidity (pN.µm²)
B
R = 7 µm
0.01 s⁻¹
0.06 s⁻¹
400 s
2 µm
Catastrophe rate
x (µm)
y (µm)
Dist. to center (µm)
Catastrophe rate (s⁻¹)
C
R = 7 µm
15 MTs
350 MTs
400 s
2 µm
MT number
x (µm)
y (µm)
Dist. to center (µm)
MT number
D
R = 7 µm No pivoting
1 pN/µm
3 pN/µm
400 s
2 µm
Gliding stiffness
x (µm)
y (µm)
Dist. to center (µm)
Gliding stiffness (pN/µm)
E
R = 7 µm No gliding
5 pN/µm
15 pN/µm
400 s
2 µm
Pivoting stiffness
x (µm)
y (µm)
Dist. to center (µm)
Pivoting sitffness (pN/µm)

Figure 6

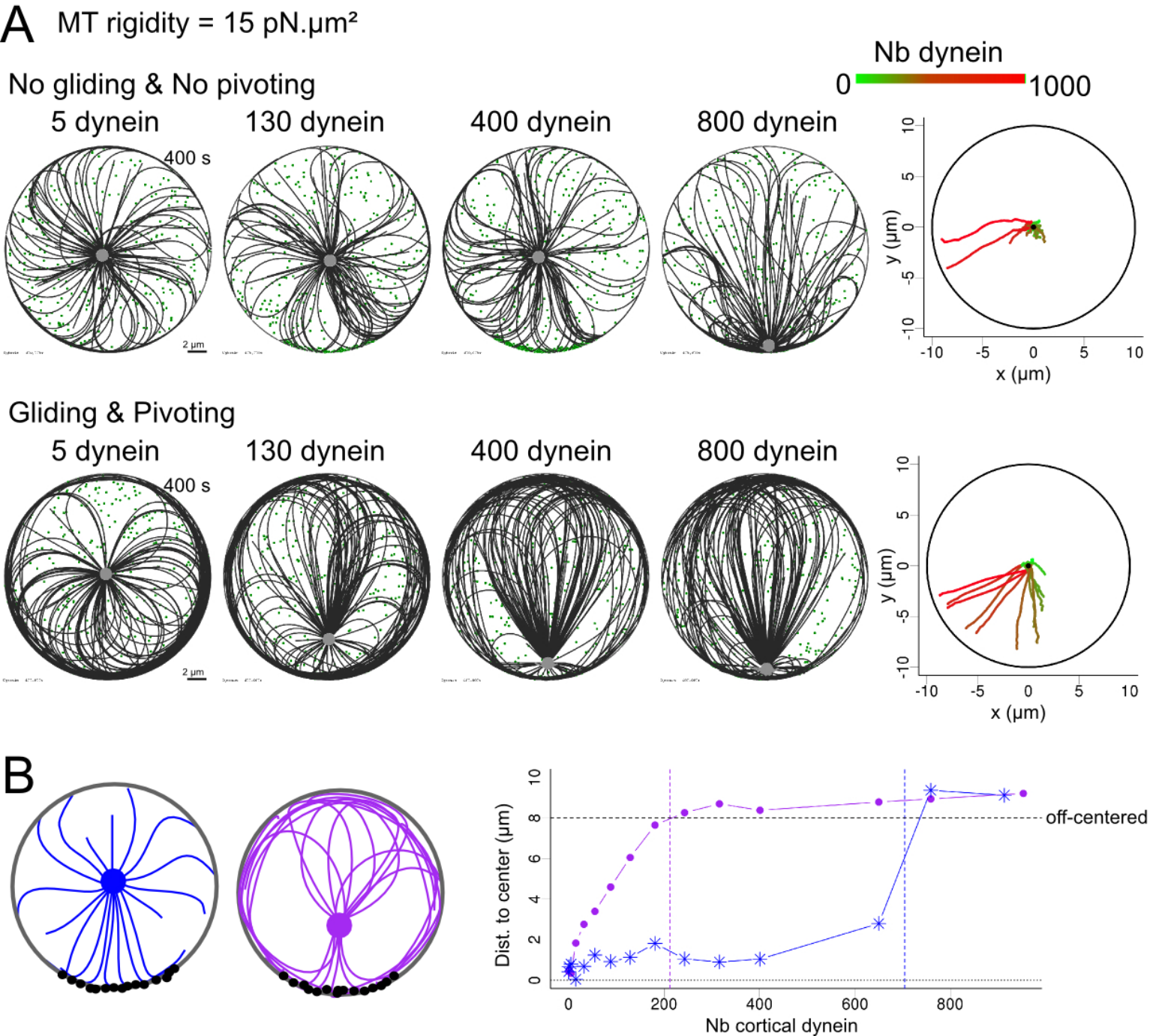
A
MT rigidity = 15 pN.µm²
Nb dynein
0
1000
No gliding & No pivoting
5 dynein
130 dynein
400 dynein
800 dynein
400 s
2 µm
y (µm)
x (µm)
Gliding & Pivoting
5 dynein
130 dynein
400 dynein
800 dynein
400 s
2 µm
y (µm)
x (µm)
B
Dist. to center (µm)
Nb cortical dynein
off-centered